Activity differences of rutile and anatase TiO_2 polymorphs in catalytic HBr oxidation

Vladimir Paunović [a,*], Marcos Rellán-Piñeiro [b], Núria López [b], Javier Pérez-Ramírez [a,*]

[a] Institute for Chemical and Bioengineering, Department of Chemistry and Applied Biosciences, ETH Zurich, Vladimir-Prelog-Weg 1, 8093, Zürich, Switzerland
[b] Institute of Chemical Research of Catalonia (ICIQ), The Barcelona Institute of Science and Technology, Av. Països Catalans 16, 43007, Tarragona, Spain

ARTICLE INFO

Keywords:
Bromine recovery
HBr oxidation
Natural gas upgrading
Titania
Rutile
Anatase

ABSTRACT

This article investigates the activity of TiO_2-rutile and TiO_2-anatase polymorphs in the catalytic HBr oxidation, which is an enabling process to close the halogen loop in bromine-mediated transformation of natural gas to high-value chemicals and liquid fuels. The evaluation of rutile-, anatase-, and rutile-anatase TiO_2 catalysts, exhibiting the variable specific surface areas, revealed that anatase phase is also active in this reaction. Nonetheless, in contrast to photocatalytic processes in which anatase is typically more active than rutile, rutile exhibits *ca.* 2–5 times higher intrinsic rates of HBr oxidation than anatase. Thereby, the apparent activation energies and reaction orders with respect to HBr, O_2, and H_2O display similar values for the two polymorphs. The activity differences were rationalized by density functional theory analysis, which showed that HBr oxidation follows a similar defect-driven mechanism over the most stable rutile (110) and anatase (101) surfaces. Herein, HBr activates the catalyst through a self-doping mechanism that involves the substitution of surface oxygen by bromine with the concomitant reduction of Ti^{4+} to Ti^{3+} centers. This forms a defect level that is placed in the band gap and allows for the O_2 activation on the catalyst surface. While the HBr adsorption and H_2O desorption display a similar energy profiles on both polymorphs, the O_2 activation and Br_2 evolution are more facile over rutile compared to anatase surface due to shorter distances between the coordinatively unsaturated Ti_{cus} sites and easier reduction of Ti^{4+} centers upon product desorption, respectively.

1. Introduction

Bromination of methane and other light alkanes coupled with the transformation of thus obtained bromoalkanes into high-value chemicals and liquid fuels by elimination of hydrogen bromide (HBr) represents an attractive catalytic route for the valorization of abundant natural gas, which could overcome the challenges related to the energy- and capital-intensiveness of existing industrial processes [1,2]. Nonetheless, a complete recovery of HBr constitutes the key prerequisite for the implementation of this technology. Heterogeneously catalyzed oxidation of HBr to bromine (Br_2) offers a realistic potential to close the halogen loop given its low energy requirements, continuous operation, and process simplicity [2–4]. However, HBr oxidation faces the major challenge of catalyst deactivation due to excessive bromination under oxygen-lean operation, which is an important process requirement that may allow for the use of air as an O_2 source [3–6]. EuOBr and TiO_2-rutile are the only active phases with proven stability under these conditions owing to their ability to limit the bromination of the catalyst bulk and surface, respectively. Thereby, TiO_2-rutile offers substantial cost advantages over EuOBr [4,6]. The striking activity of TiO_2-rutile in HBr oxidation, which contrasts its inability to catalyze a congeneric HCl to Cl_2 oxidation (Deacon reaction), was rationalized by a self-doping with bromine and consequent formation of defect Ti states enabling O_2 activation [6,7].

Besides rutile, anatase is another stable polymorph of TiO_2, which finds much broader application as a photocatalyst or catalyst support [8–10]. Similar to rutile, anatase exhibits tetragonal crystalline geometry [10]. Nonetheless, the angles between the Ti-O bonds of anatase are more distorted from 90 degrees. These configurational differences result in a larger band gap (3.2 eV *vs.* 3 eV) and lower thermal stability of anatase as compared to rutile [8,9]. However, specific surface areas attainable by anatase are typically higher than for rutile, which is of great interest for (photo)catalytic applications [9]. In fact, anatase and anatase-rutile mixtures (*e.g.*, P25) display a higher photocatalytic activity than rutile [9–11]. However, although fundamentally and practically relevant, the activities of anatase and anatase-rutile mixtures in

* Corresponding authors.
E-mail addresses: vladimir.paunovic@chem.ethz.ch (V. Paunović), jpr@chem.ethz.ch (J. Pérez-Ramírez).

HBr oxidation have not been studied yet.

Herein, we systematically investigated the HBr oxidation kinetics and structural stability of rutile, anatase, and rutile-anatase catalysts exhibiting low and high surface areas under practically relevant conditions in order to assess the inherent activity differences between TiO_2 polymorphs. The experimental findings are corroborated by the state-of-the-art density functional theory (DFT) simulations that rationalize the structural and electronic descriptors governing the observed performances. We show that anatase displays a substantial activity and structural stability in this reaction, as corroborated by X-ray diffraction, N_2 sorption, and Raman spectroscopy analysis of the used catalysts. Furthermore, kinetic and DFT analysis indicate the same defect driven mechanism of HBr oxidation over both rutile and anatase surfaces. Nonetheless, the O_2 activation and rate-limiting Br_2 evolution are less impeded on the rutile surface due to geometrical factors and easier reduction of Ti^{4+} cations, respectively, which ultimately leads to higher intrinsic rates over rutile as compared to anatase.

2. Experimental details

Commercially available TiO_2-rutile: TiO_2-r-n (Aldrich, 99.9 %), TiO_2-r-b (ABCR, 99.8 %), TiO_2-r-h (Alfa Aesar, 99.998 %), TiO_2-r-s (Strem, 99.9 %), TiO_2-anatase: TiO_2-a-n (Aldrich, 99.7 %), TiO_2-a-e (Alfa Aesar, 99.8 %), and TiO_2-P25: TiO_2-ar-P25 (Acros, 99.9 %) were calcined at 773 K for 5 h (heating rate 5 K min^{-1}) prior to their use in HBr oxidation.

Powder X-ray diffraction (XRD) was measured using a PANalytical X'Pert PRO-MPD diffractometer with Bragg-Brentano geometry by applying Cu Kα radiation (λ =1.54060 Å). The data were recorded in the 2θ range of 10-70° with an angular step size of 0.05° and a counting time of 1.8 s per step. N_2 sorption at 77 K was performed using a Micromeritics TriStar analyzer. Prior to the measurement, the sample (0.5 g) was evacuated to 50 mbar at 573 K for 12 h. Raman spectroscopy was performed on a WITec CRM200 confocal Raman system comprising a 532 nm laser, a 100× objective lens with numerical aperture NA = 0.9 (Nikon Plan), and a fiber-coupled grating spectrometer (2400 lines per mm). The spectra were recorded using a laser power of 10 mW in the Raman shift range of 100-1000 cm^{-1} by co-adding 5 accumulations at spectral sampling resolution of 0.7 cm^{-1} and acquisition time of 1−5 s. Temperature-programmed reduction with hydrogen (H_2-TPR) was conducted in a Micromeritics Autochem II 2920 unit equipped with a thermal conductivity detector. The sample (0.2 g) was loaded in an U-shaped quartz reactor between two plugs of quartz wool and pretreated in He (20 cm^3 STP min^{-1}) at 573 K for 1 h. H_2-TPR was then conducted by feeding the H_2 in N_2 gas mixture (5 mol.% H_2, 20 cm^3 min^{-1}) in the temperature range of 350-1000 K using a heating rate of 10 K min^{-1}.

HBr oxidation tests were performed in a continuous-flow fixedbed reactor setup [4]. A catalyst was placed in a quartz reactor tube (inner diameter, d_r =8 mm) between two plugs of quartz wool and the tip of the quartz thermowell accommodating a thermocouple was positioned in the middle of the bed. The bed was heated to the desired temperature under He flow and was left to stabilize for at least 30 min under these conditions prior to admitting the reaction mixture comprising HBr (Air Liquide, purity 2.8, anhydrous), O_2 (PanGas, purity 5.0), deionized water, and He (PanGas, purity 5.0; used as carrier gas). Unless otherwise stated, the catalytic runs were conducted using a water-free inlet gas mixture with a molar ratio of HBr:O_2:He = 10:2.75:87.25, total gas flow of F_T = 100 cm^3 min^{-1}, and a catalyst weight of W_{cat} =0.5 g (particle size, d_p = 0.20.4 mm) in the temperature range of T = 548-675 K and at total pressure of P = 1 bar. The production of bromine was quantified by passing the outlet reactor feed through an impinging bottle filled with 0.1 M KI aqueous solution ($Br_2 + 3I^- \rightarrow I_3^- + 2Br^-$) followed by iodometric titration (Mettler Toledo G20 Compact Titrator) of the formed triiodide ($I_3^- + 2S_2O_3^{2-} \rightarrow 3I^- + S_4O_6^{2-}$) with 0.01 M $Na_2S_2O_3$ (Aldrich, 99.99 %). The conversion of HBr and the rate normalized per surface area, r_s, were calculated using Equations. 1-2, respectively, where n(HBr)^{inlet} and n(Br_2)^{outlet} are the molar flow of HBr and Br_2 at reactor inlet and outlet, respectively. Mass- and heat-transfer limitations can be excluded based on the evaluation of theoretical criteria suggested by Carberry, Mears, and Weisz-Prater, and constant conversion level for the particle size varied between 0.1-0.6 mm [12].

$$X_{HBr} = \frac{2 \times n_{Br_2}^{outlet}}{n_{HBr}^{inlet}} \times 100, \% \quad (1)$$

$$r_S = \frac{n_{Br_2}^{outlet}}{S_{BET} \times W_{cat}} \times 100, \ \ mol_{Br_2}\, s^{-1} m^{-2} \quad (2)$$

2.1. Computational details

Density Functional Theory (DFT) calculations were performed with the Vienna ab Initio Simulation Package (VASP), version 5.4.4 [13]. Within the Generalized Gradient Approximation (GGA), exchange-correlation energy was described by Perdew-Burke-Ernzerhof (PBE) functional and the van der Waals interactions were accounted with Grimme's semiempiric D3 method [14]. The on-site Coulomb interactions of 3d electrons of Ti were described with the Hubbard U correction with U_{eff}=4.2 eV [15]. The inner electrons were described with projector-augmented wave (PAW) pseudopotentials (with 12 valence electrons for Ti atoms), whereas the valence electrons were expanded in plane waves with cutoff energy of 500 eV [16]. Spin-polarized calculations were performed for system with unpaired electrons.

Rutile and anatase bulks were optimized with 9 × 9 × 15 and 9 × 9 × 5 k-point mesh, respectively, and a cutoff energy of 800 eV. Surface calculations were performed using slab models. Due to asymmetry of the slabs the dipole correction was used to avoid the spurious terms [17]. Calculations were performed on the most stable rutile (110) and anatase (101) surfaces, since they are the main exposed planes in TiO_2 nanoparticles as is shown by the Wulff construction models for rutile and anatase phases (Supplementary information, **Table S1** and **Fig. S1**). A (3 × 2) supercell with five layers with 5 × 3 × 1 k-point sampling was considered for rutile (110), and a (1 × 3) supercell with 3 × 3 × 1 k-point sampling and four layers was examined for anatase (101). Adsorbates and three (two) topmost layers for rutile (anatase) were allowed to relax. Reaction steps are either barrierless or have negligible energy barriers and, therefore, only its thermodynamics is commented along this work. All the calculated structures are presented in Supplementary information (**Fig. S2**) and are also published in the ioChem-BD database [18].

3. Results and discussion

X-ray diffraction analysis confirmed the presence of pure rutile phase in TiO_2-r-n, TiO_2-r-b, TiO_2-r-p, and TiO_2-r-s, pure anatase phase in TiO_2-a-n and TiO_2-a-e, and a mixture of anatase and rutile phases in approximate weight ratio of 7:3 in TiO_2-ar-P25 (Fig. 1a). Thereby, TiO_2-r-n, TiO_2-a-n, TiO_2-ar-P25, and TiO_2-a-e exhibit smaller crystallite sizes and large specific surface areas, whereas TiO_2-r-b, TiO_2-r-s, and TiO_2-r-p display relatively large crystallites and small surface areas. Consistent with crystallographic analysis, Raman spectra of TiO_2-r-n, TiO_2-r-b, TiO_2-r-s, and TiO_2-r-p showed characteristic multiphonon (235 cm^{-1}), E_g (443 cm^{-1}), and A_{1g} (608 cm^{-1}) modes of rutile, while the spectra of TiO_2-a-n, TiO_2-a-e, and TiO_2-ar-P25 unveiled the $E_{g(1)}$ (141 cm^{-1}), $B_{1g(1)}$ (397 cm^{-1}), A_{1g} (514 cm^{-1}), and $E_{g(3)}$ (638 cm^{-1}) modes of anatase (Fig. 1b) [9,19]. Thereby, TiO_2-ar-P25 catalyst displayed only the bands of anatase, which can be explained by a larger fraction and higher Raman intensity of this phase as compared to rutile.

The activity of TiO_2 catalysts was assessed in the temperature range of 548−673 K using an inlet feed that contained HBr and O_2 in a molar ratio of HBr:O_2 = 10:2.75, *i.e.*, a small O_2 excess (10 mol.%) with respect to the reaction stoichiometry. These conditions reflect the industrially attractive operation regime [4]. Characterization of catalysts used in

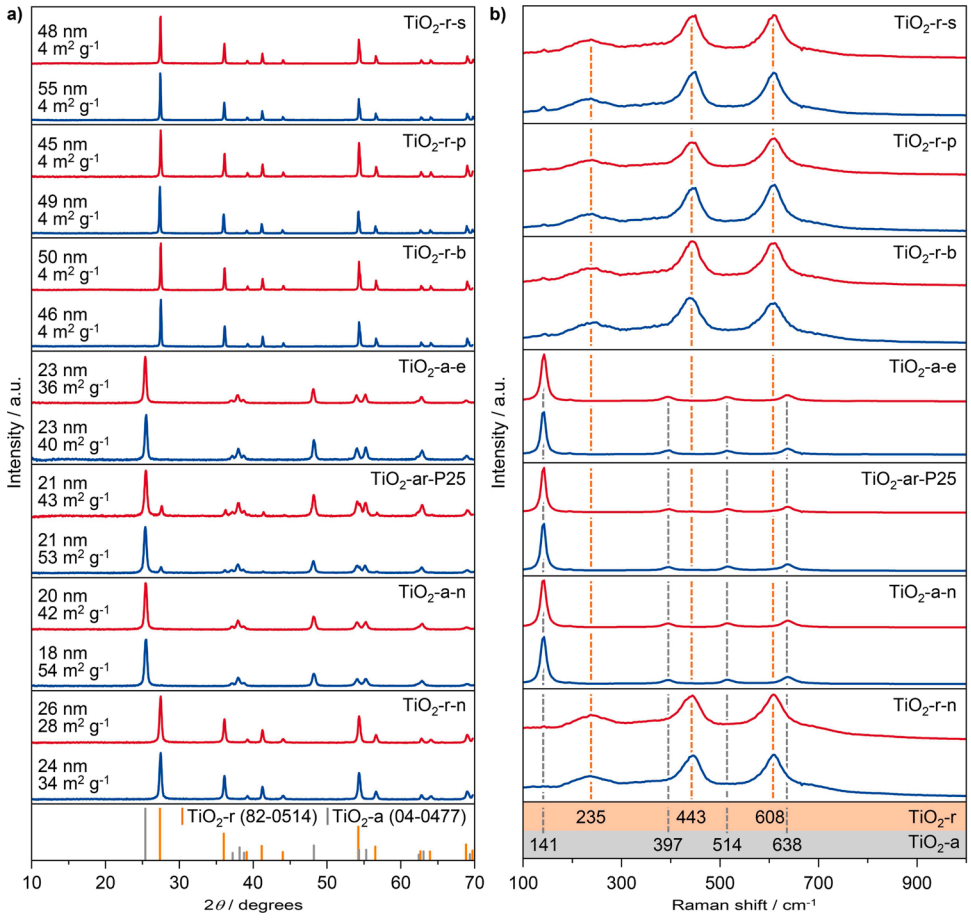

Fig. 1. a) X-ray diffractograms and b) Raman spectra of TiO_2 catalysts in fresh form (blue) and after HBr oxidation (red). The average crystallite size and total surface areas of the catalysts are displayed above the respective diffractograms. The reference diffraction patterns of TiO_2-rutile and TiO_2-anatase phases are presented below the measured diffractograms with their ICDD-PDF numbers. (For interpretation of the references to colour in this figure legend, the reader is referred to the web version of this article).

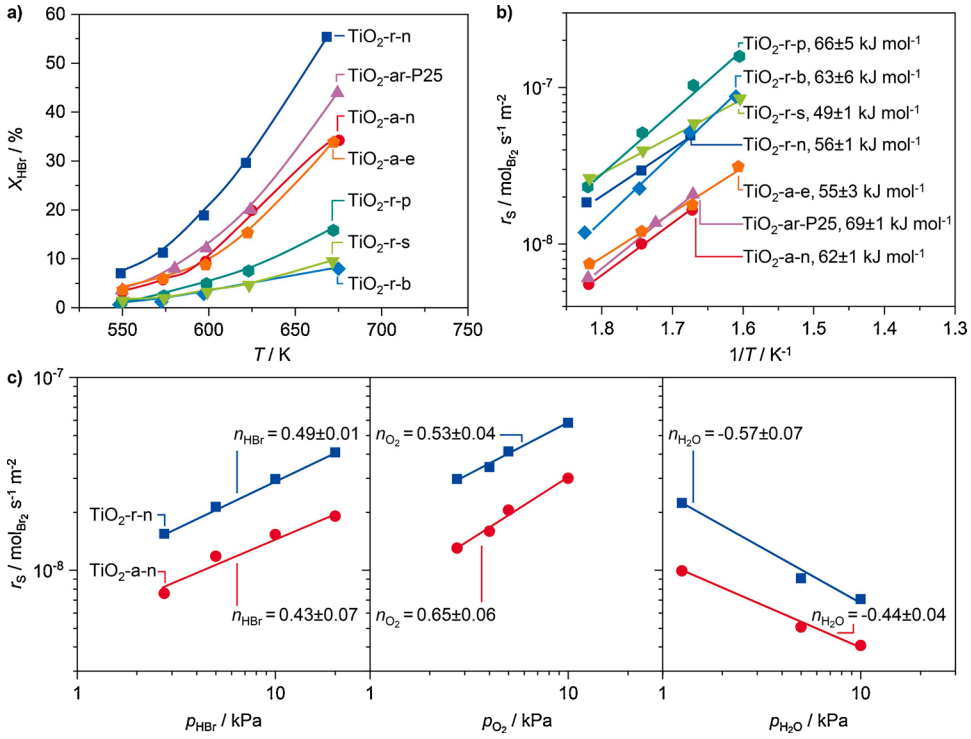

Fig. 2. a) Conversion of HBr *versus* temperature and b) surface-normalized reaction rates *versus* reciprocal temperature for TiO_2 catalysts. c) Surface-normalized reaction rates over TiO_2-r-n and TiO_2-a-n *versus* partial pressure of HBr (left), O_2 (middle), and H_2O (right). The apparent activation energies and reaction orders are provided in b) and c), respectively. Conditions: a,b) HBr:O_2:He = 10:2.75:87.25 and T = 548-675 K, c) HBr:O_2:H_2O:He = 2.75-20:2.75:0:94.5-77.25 (HBr variation), 10:2.75-10:0:87.87.25-80 (O_2 variation), or 10:2.75:1.5-10:85.75-77.25 (H_2O variation), and T =573 K (TiO_2-r-n) or 596 K (TiO_2-a-n). In a) and b) temperature was varied from the lowest to the highest value. All tests were performed at P = 1 bar using W_{cat} = 0.5 g and F_T = 100 cm^3 min^{-1}.

catalytic tests showed that the original phase composition was preserved, although the high-surface area materials displayed a small increase of crystallite size coupled with a small-to-medium drop in S_{BET} (Fig. 1). The results corroborate the structural stability of both TiO_2 polymorphs under O_2-lean conditions, in good correspondence with previous studies on TiO_2-rutile [6,7].

Notably, the anatase-containing TiO_2-a-n, TiO_2-a-e, and TiO_2-ar-P25 catalysts displayed a substantial Br_2 production, thus demonstrating that the activity of TiO_2 is not only limited to its rutile polymorph (Fig. 2a). Thereby, the highest conversions of HBr were attained over high-surface area materials, which evidences the positive impact of TiO_2 dispersion on the rate of HBr oxidation. Nonetheless, TiO_2-r-n displays *ca.* 1.5-2 times higher conversion levels than TiO_2-a-n, TiO_2-a-e, and TiO_2-ar-P25, although its specific surface area is lower than in the case of these materials. In addition, the light-off curve of TiO_2-ar-P25, which contains anatase and a small fraction of rutile, is positioned between those of anatase-based TiO_2-a-n and rutile-based TiO_2-r-n materials. This aspect was further analyzed by comparing the rates normalized per S_{BET} of the pre-equilibrated materials, which can be considered as a measure of the intrinsic catalyst activity. Notably, the rates observed over rutile were *ca.* 2-5 times higher as compared to anatase systems. Nonetheless, the apparent activation energies measured over all materials displayed very similar values (Fig. 2b). Further evaluation of HBr oxidation kinetics over representative TiO_2-r-n and TiO_2-a-n catalysts showed that they exhibit similar apparent reaction orders with respect to HBr, O_2, and H_2O. The kinetic analysis thus provides hints that the reaction mechanism is likely similar for two polymorphs (Fig. 2c).

DFT analysis of the HBr oxidation activity of the most stable rutile (110) and anatase (101) surfaces were undertaken to rationalize the performance differences observed in HBr oxidation. The mechanism of this reaction on rutile (110) surface comprises a sequence of acid-base and redox steps, which require two types of active sites: the five-fold coordinated titania centers (Ti_{cus}, cus stands for coordinatively unsaturated sites) and bridge oxygens (O_b) that are bonded to two Ti centers [7]. The reaction centers that are analogues to Ti_{cus} and O_b are also present on anatase (101) surface (Fig. 3a). However, Ti_{cus}-Ti_{cus} distance in the case of rutile (3.014 Å along the [001] direction) is smaller than in anatase (3.856 Å along [010] direction). Another relevant difference between the polymorphs is their calculated band gap energy of 2.03 eV for rutile and 2.22 eV for anatase. These values are lower than the experimental ones (3.03 and 3.20 eV, respectively) due to the use of GGA functionals, which are known to underestimate the band gaps [20]. Nonetheless, this is a systematic error that does not affect the drawn conclusions as the difference between the band gap energies (0.19 eV) is essentially identical to the experimentally observed value (0.17 eV). The valence band of pristine TiO_2 phases is placed at much lower energy than the lowest unoccupied molecular orbital (LUMO) of O_2, thus resulting in very endothermic activation of O_2 (> 4 eV) [7]. Nonetheless, the adsorption of HBr leads to substitution of O_b sites with bromine centers (Br_b), *i.e.*, to the formation of self-doped $TiO_2(Br_b)$ (Fig. 3a, right). Thereby, the final system is extrinsically doped since the replacement of O_b for a Br_b leaves an extra electron, which reduces a Ti^{4+} center to Ti^{3+}. The bromine doping is similarly exothermic (*ca.* 1.40 eV) for both phases. However, the most stable Ti^{3+} center is located underneath the surface for rutile and at the surface for anatase (Fig. 3a, right) [21,22]. Self-doping of TiO_2 introduces a defect level in the band gap that enables exothermic O_2 activation (Fig. 3b) [23,24]. When there is only one defect level in the supercell calculation, O_2 adsorbs in the form of superoxo species (O_2^-). This process is exothermic on both rutile (-0.90 eV) and anatase (-1.18 eV). Further activation of the O_2 requires more defect electrons and results in the formation of dihapto peroxo states, with energy change of -1.45 eV and -1.42 eV for rutile and anatase, respectively. The lower stabilization in the case of the anatase is due to the geometric constraints on the surface (longer Ti_{cus}-Ti_{cus} distance). The dihapto O_2 bonded to two Ti_{cus}, then dissociates to form the reactive O_{cus} species. The next reaction steps comprise HBr adsorption

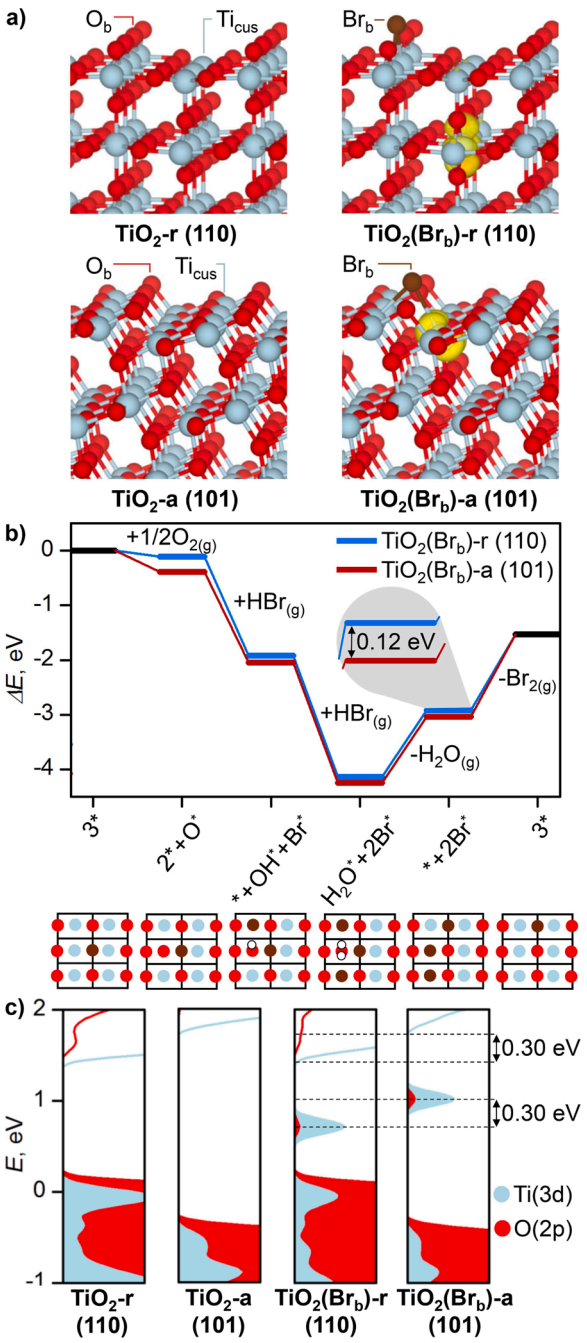

Fig. 3. a) Optimized structure of pristine TiO_2-rutile (110) and TiO_2-anatase (101), doped $TiO_2(Br_b)$-rutile (110) and $TiO_2(Br_b)$-anatase (101), and calculated spin density for doped systems at 0.03 $Å^2$. b) Reaction energy profile for HBr oxidation on $TiO_2(Br_b)$-rutile (110) and $TiO_2(Br_b)$-anatase (101) surfaces. Corresponding surface states are defined and schematically depicted bellow the profile. Ti_{cus} sites are indicated with *. c) Aligned density of states (DOS) of pristine and doped surfaces. Color code in a) and b): Ti: light blue; O: red; Br: brown; H: white; calculated spin density: yellow. (For interpretation of the references to colour in this figure legend, the reader is referred to the web version of this article).

coupled with O_{cus} protonation, followed by -O_{cus}H recombination and H_2O_{cus} desorption, which given the comparable acid-base properties of two phases, display similar energy profile (Fig. 3b). These results are consistent with the experimentally observed similar apparent reaction orders with respect to HBr, O_2, and H_2O (Fig. 2c). The most energy demanding step for HBr oxidation over both rutile and anatase surfaces

involves the recombination of Br atoms adsorbed on neighboring Ti centers to form Br_2. Br_2 desorption leaves one electron on the surface that reduces a Ti^{4+} center, *i.e.*, the electron is transferred to the defect level in an endothermic process. The aligned band structures of rutile and anatase show that the energy of the defect level of rutile is *ca.* 0.30 eV lower than for anatase (Fig. 3c) [25]. However, adsorbed Br_2 that interacts with two Ti_{cus} cations is more destabilized in anatase, due to the larger distance between the neighboring Ti_{cus} sites. As a result, the energy of bromine desorption over rutile (1.39 eV) is only 0.12 eV lower than for anatase (1.51 eV). The smaller energy barrier (Fig. 3b, inset) for Br_2 evolution is another factor that favours the higher intrinsic activity of rutile.

In overall, geometric and electronic terms are responsible for the different activity of rutile and anatase polymorphs. Geometric effects enhance O_2 activation on rutile compared to anatase surface. In particular, although the superoxo and monohapto species are nicely trapped on the anatase surface (more exothermic process than on rutile) and the energy difference for the adsorption on both surfaces overlaps with the energy difference between the Ti^{3+} states in two materials, the geometric frustration in the dihapto adsorption induced by the larger Ti_{cus}-Ti_{cus} distance on anatase inverts the binding energy trend. The electronic contribution comes from the lower energy position of the Ti^{3+} states in rutile, which reduces the energy for reintroducing the electron to the material upon Br_2 elimination. Hence, the higher activity of rutile over anatase is related to a higher propensity of the former phase to localize the electrons, *i.e.*, to its more facile reducibility. This outcome of DFT analysis is also consistent with the lower temperature onset of TiO_2-r-n compared to TiO_2-a-n as determined by H_2-TPR (Fig. 4).

4. Conclusions

We showed that TiO_2-anatase displays significant activity and structural stability in HBr oxidation, although its intrinsic rates are lower as compared to TiO_2-rutile polymorph. Kinetics and DFT analyses indicate that two polymorphs exhibit essentially identical reaction mechanism. Herein, HBr adsorption causes surface-confined bromination that generates the defect Ti^{3+} states associated with defect level in the band gap, which enables O_2 activation and facilitates bromine evolution. A higher activity of rutile is a consequence of (*i*) geometric parameters that facilitate O_2 activation on rutile due to shorter Ti_{cus}-Ti_{cus} distance, and lead to a higher stabilization of dihapto-adsorbed O_2, and (*ii*) electronic parameters that enhance Br_2 evolution due to the lower energy of the defect level in rutile, which renders the electron transfer less endothermic compared to anatase.

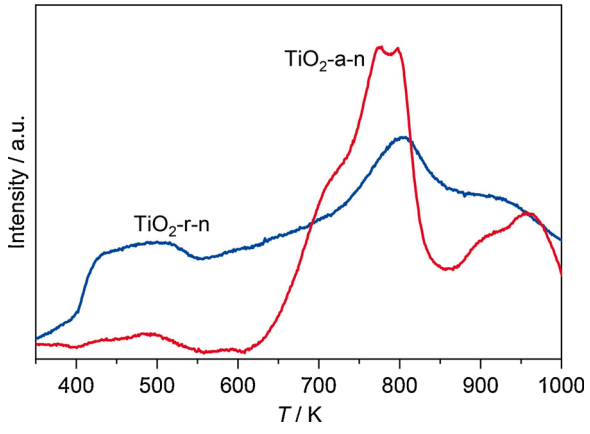

Fig. 4. Temperature-programmed reduction with H_2 over TiO_2-r-n and TiO_2-a-n catalysts. Conditions: H_2:N_2 = 5:95, T = 350-1000 K, W_{cat} = 0.2 g, F_T = 20 cm^3 min^{-1}, and P = 1 bar.

Declaration of Competing Interest

The authors declare that they have no known competing financial interests or personal relationships that could have appeared to influence the work reported in this paper.

CRediT authorship contribution statement

Vladimir Paunović: Conceptualization, Data curation, Formal analysis, Methodology, Writing - original draft. **Marcos Rellán-Piñeiro:** Formal analysis, Methodology, Visualization. **Núria López:** Formal analysis, Methodology, Supervision, Writing - review & editing. **Javier Pérez-Ramírez:** Conceptualization, Funding acquisition, Supervision, Writing - original draft, Writing - review & editing.

Acknowledgements

ETH Zurich is acknowledged for financial support. Prof. Ralph Spolenak from ETH Zurich is acknowledged for the access to Raman spectrometer.

References

[1] E. McFarland, Unconventional chemistry for unconventional natural gas, Science 338 (2012) 340–342.
[2] R. Lin, A.P. Amrute, J. Pérez-Ramírez, Halogen-mediated conversion of hydrocarbons to commodities, Chem. Rev. 117 (2017) 4182–4247.
[3] M. Moser, L. Rodríguez-García, A.P. Amrute, J. Pérez-Ramírez, Catalytic bromine recovery: an enabling technology for emerging alkane functionalization processes, ChemCatChem 5 (2013) 3520–3523.
[4] V. Paunović, R. Lin, M. Scharfe, A.P. Amrute, S. Mitchell, R. Hauert, J. Perez-Ramírez, Europium oxybromide catalysts for efficient bromine looping in natural gas valorization, Angew. Chem. Int. Ed. 56 (2017) 9791–9795.
[5] M. Moser, G. Vilé, S. Colussi, F. Krumeich, D. Teschner, L. Szentmiklósi, A. Trovarelli, J. Pérez-Ramírez, Structure and reactivity of ceria-zirconia catalysts for bromine and chlorine production via the oxidation of hydrogen halides, J. Catal. 331 (2015) 128–137.
[6] M. Moser, V. Paunović, Z. Guo, L. Szentmiklósi, M.G. Hevia, M. Higham, N. López, D. Teschner, J. Pérez-Ramírez, Interplay between surface chemistry and performance of rutile-type catalysts for halogen production, Chem. Sci. 7 (2016) 2996–3005.
[7] M. Moser, I. Czekaj, N. López, J. Pérez-Ramírez, The virtue of defects: stable bromine production by catalytic oxidation of hydrogen bromide on titanium oxide, Angew. Chem. Int. Ed. 53 (2014) 8628–8633.
[8] D.A.H. Hanaor, C.C. Sorrell, Review of the anatase to rutile phase transformation, J. Mater. Sci. 46 (2011) 855–874.
[9] X. Chen, S.S. Mao, Titanium dioxide nanomaterials: synthesis, properties, modifications and applications, Chem. Rev. 107 (2007) 2891–2959.
[10] U. Diebold, The surface science of titanium dioxide, Surf. Sci. Rep. 48 (2003) 53–229.
[11] T. Luttrell, S. Halpegamage, J. Tao, A. Kramer, E. Sutter, M. Batzill, Why is anatase a better photocatalyst than rutile? Model studies on epitaxial TiO_2 films, Sci. Rep. 4 (2015) 1–8.
[12] F. Kapteijn, J.A. Moulijn, Laboratory testing of solid catalysts, in: G. Ertl, H. Knözinger, in: F. Schüth, J. Weitkamp (Eds.), Handbook of Heterogeneous Catalysis, Wiley-VCH, Weinheim, 2008, pp. 2019–2045.
[13] G. Kresse, J. Furthmüller, Efficiency of ab-initio total energy calculations for metals and semiconductors using a plane-wave basis set, Comput. Mater. Sci. 6 (1996) 15–50.
[14] S. Grimme, J. Antony, S. Ehrlich, H. Krieg, A consistent and accurate ab initio parametrization of density functional dispersion correction (DFT-D) for the 94 elements H-Pu, J. Chem. Phys. 132 (2010), 154104.
[15] S. Dudarev, G. Botton, Electron-energy-loss spectra and the structural stability of nickel oxide: an LSDA+U study, Phys. Rev. B 57 (1998) 1505–1509.
[16] G. Kresse, D. Joubert, From ultrasoft pseudopotentials to the projector augmented-wave method, Phys. Rev. B 59 (1999) 1758–1775.
[17] G. Makov, M.C. Payne, Periodic boundary conditions in ab initio calculations, Phys. Rev. B 51 (1995) 4014–4022.
[18] M. Álvarez-Moreno, C. De Graaf, N. López, F. Maseras, J.M. Poblet, C. Bo, Managing the computational chemistry big data problem: the ioChem-BD platform, J. Chem. Inf. Model. 55 (2015) 95–103.

[19] O. Frank, M. Zukalova, B. Laskova, J. Kürti, J. Koltai, L. Kavan, Raman spectra of titanium dioxide (anatase, rutile) with identified oxygen isotopes (16, 17, 18), Phys. Chem. Chem. Phys. 14 (2012) 14567–14572.
[20] S. Lutfalla, V. Shapovalov, A.T. Bell, Calibration of the DFT/GGA+U method for determination of reduction energies for transition and rare earth metal oxides of Ti, V, Mo, and Ce, J. Chem. Theory Comput. 7 (2011) 2218–2223.
[21] B.J. Morgan, G.W. Watson, A DFT + U description of oxygen vacancies at the TiO_2 rutile (110) surface, Surf. Sci. 601 (2007) 5034–5041.
[22] M.A. Ha, A.N. Alexandrova, Oxygen Vacancies of Anatase(101): extreme sensitivity to the density functional theory method, J. Chem. Theory Comput. 12 (2016) 2889–2895.
[23] M.D. Rasmussen, L.M. Molina, B. Hammer, Adsorption, diffusion, and dissociation of molecular oxygen at defected TiO_2(110): a density functional theory study, J. Chem. Phys. 120 (2004) 988–997.
[24] S. Selcuk, A. Selloni, Facet-dependent trapping and dynamics of excess electrons at anatase TiO_2 surfaces and aqueous interfaces, Nat. Mater. 15 (2016) 1107–1112.
[25] D.O. Scanlon, C.W. Dunnill, J. Buckeridge, S.A. Shevlin, A.J. Logsdail, S. M. Woodley, C.R.A. Catlow, M.J. Powell, R.G. Palgrave, I.P. Parkin, G.W. Watson, T.W. Keal, P. Sherwood, A. Walsh, A.A. Sokol, Band alignment of rutile and anatase TiO_2, Nat. Mater. 12 (2013) 798–801.